HHS Public Access

Author manuscript

Mult Scler. Author manuscript; available in PMC 2022 March 05.

Published in final edited form as:

Mult Scler. 2022 March ; 28(3): 393–405. doi:10.1177/13524585211023343.

Association of retinal atrophy with cortical lesions and leptomeningeal enhancement in multiple sclerosis on 7T MRI

Ryan Mizell[1,2], **Hegang Chen**[3], **Jeffrey Lambe**[4], **Shiv Saidha**[4], **Daniel M. Harrison**[1,2,4,5]

[1]Baltimore VA Medical Center, Baltimore, MD

[2]University of Maryland Medical Center, Baltimore, MD

[3]Department of Epidemiology and Public Health, University of Maryland School of Medicine of Neurology, MD

[4]Johns Hopkins University School of Medicine, Baltimore, MD

[5]Department of Neurology, University of Maryland School of Medicine, Baltimore, MD

Abstract

Background: Retinal atrophy in multiple sclerosis (MS) measured by optical coherence tomography (OCT) correlates with demyelinating lesions and brain atrophy, but its relationship with cortical lesions (CLs) and meningeal inflammation is not well known.

Objectives: To evaluate the relationship of retinal layer atrophy with leptomeningeal enhancement (LME) and CLs in MS as visualized on 7 Tesla (7T) MRI.

Methods: Forty participants with MS underwent 7T MRI of the brain and OCT. Partial correlation and mixed effects regression evaluated relationships between MRI and OCT findings.

Results: All participants had CLs and 32 (80%) participants had LME on post-contrast MRI. Ganglion cell/inner plexiform layer (GCIPL) thickness correlated with total CL volume ($r=-0.45$, $p < 0.01$). Participants with LME at baseline had thinner mRNFL ($p = 0.01$) and GCIPL ($p < 0.01$). Atrophy in various retinal layers were faster in those with certain patterns of LME. For example, mRNFL declined −1.113 [−1.974, −0.252] μm/year faster in those with spread/fill pattern LME foci at baseline compared to those without ($p=0.01$).

Conclusion: This study associates MRI findings of LME and cortical pathology with thinning of retinal layers as measured by OCT, suggesting a common link between meningeal inflammation, CLs, and retinal atrophy in MS.

Keywords

7 Tesla; MRI; multiple sclerosis; leptomeningeal enhancement; meningeal inflammation; retinal atrophy; optical coherence tomography

Corresponding Author: Daniel M. Harrison, MD., 110 South Paca Street, Baltimore, Maryland, 21204, dharrison@som.umyaryland.edu.

Introduction

The importance of cortical and meningeal pathology to the disease processes of multiple sclerosis (MS) is increasingly recognized. Cortical pathology is common and comprises both cortical atrophy and distinct cortical lesions (CLs). CLs tend to be less inflammatory than white matter lesions (WMLs) [1, 2] and are implicated in worsening disability and cognition.[3, 4] The presence of cortical pathology appears to be particularly prominent in the progressive phase of MS, especially with regard to the subpial CL subtypes.[4, 5]

Lymphoid aggregates in the leptomeninges are found within 40–50% of patients with secondary progressive MS (SPMS) and subpial CLs are found in close proximity to leptomeningeal inflammation at autopsy.[6–8] Leptomeningeal contrast enhancement (LME) is suggested as an imaging surrogate of meningeal inflammation in MS, and its presence is associated with progressive cortical atrophy.[9, 10] Although multiple imaging studies confirm relationships between LME and reduced cortical volume and/or thickness,[9–11] it remains unclear from *in vivo* work if meningeal inflammation directly contributes to focal CL development, or is part of the general inflammatory response that leads to widespread neuronal loss and subsequent atrophy. Recent work imaging LME on 7 Tesla (7T) MRI has shown conflicting results, with one study showing no relationship between LME and CLs[11] and another showing a strong relationship between these imaging findings.[12]

Integration of optical coherence tomography (OCT) into imaging studies evaluating the broader CNS consequences of meningeal inflammation and cortical pathology may help shed further light on this process. Evaluations of the optic nerve and retina by OCT provide an opportunity for direct evaluations of the consequence of neurologic disorders on unmyelinated components of the CNS. Patients with MS have ongoing retinal atrophy that correlates with brain atrophy and can be used to predict long-term disability.[13, 14]

We sought to evaluate retinal layer thicknesses derived from OCT in MS patients in comparison to MRI evaluations of LME and cortical pathology, with the underlying hypothesis that meningeal inflammation is not just associated with local focal lesion development, but represents a pathobiological marker that is associated with widespread neuronal loss in MS. To better accomplish, we utilized 7T MRI, given the known marked increase in sensitivity to both CLs and LME at ultra-high field.[15, 16]

Methods

Protocols and Consents

Research protocols were approved by the Institutional Review Boards at the Johns Hopkins University School of Medicine, the Kennedy Krieger Institute, and the University of Maryland School of Medicine. Prior to collection of data, patients read and signed an informed consent document.

Participants

Data for this analysis was taken from a prospective observational study in which participants undergo annual study visits for clinical data collection, disability scales, 7T MRI, and OCT.

Data from this study and additional cohort and protocol details can be found in multiple prior publications.[11, 16, 17] Inclusion criteria include: ages 18 to 65 and a diagnosis of relapsing remitting (RRMS), SPMS, or primary progressive MS (PPMS) according to the 2010 McDonald Criteria,[18] with exclusion for contraindications to MRI or gadolinium. Subjects were chosen for cross-sectional analyses if baseline MRI and OCT images were available and of sufficient quality for review and for longitudinal analyses if OCT images were available from > 1 annual study visit.

MRI Protocol

MRI of the brain was performed on a 7T Philips Achieva scanner. Detailed hardware information and acquisition parameters for magnetization prepared 2 rapid acquisition gradient echo (MP2RAGE) and magnetization prepared fluid attenuated inversion recovery (MPFLAIR) images are found in the MRI appendix (Supplemental). MP2RAGE and MPFLAIR images were acquired both before and after contrast administration.

MRI Processing and Analysis

MRI processing utilized Medical Image Processing, Analysis, and Visualization (MIPAV) version 7.2, (http://mipav.cit.nih.gov), Java Image Science Toolkit (JIST) version 3.0, (https://www.nitrc.org/projects/jist), FMRIB Software Library (FSL; Oxford University), and MatLab (Mathworks). MP2RAGE was processed for a T1-weighted (T1-w) image and T1 map.[19] Generation of a denoised T1-w image was performed by multiplying the second inversion-time image in the MP2RAGE acquisition (after inhomogeneity correction) and the corresponding T1-w image. MPFLAIR images were registered to the denoised T1-w image, which was also used for skull stripping. WML identification and brain segmentation were performed as described in Spini et al.[17]

The method for identification of CLs on MP2RAGE images (Figure 1) is described in previous publications.[11, 20] Briefly, regions of cortical hypointensity were delineated on the T1-weighted (T1-w) MP2RAGE image and MPFLAIR was used for confirmation. These lesions were further classified into leukocortical, intracortical, or subpial.[1, 3] Lesions noted in hippocampal GM were classified as hippocampal CLs. Hand-drawn masks of the CLs were created with semi-automated region-growing paint tools in MIPAV.

Our methods for identification and classification of foci of LME on 7T MRI (Figure 1) have previously been described in detail.[11, 16] Briefly, subtraction MPFLAIR images (post-contrast minus pre-contrast) were reviewed alongside post-contrast MPFLAIR images and hyperintensities on post-contrast images only, found in the subarachnoid space, and were classified as LME. LME foci were classified as “nodular” (restricted to one small, spherical shaped region) or “spread/fill” (amorphous in shape, spread into the subarachnoid space and/or filling a sulcus). Spread/fill foci were further subdivided into those found within sulci (“spread/fill-sulcal”), between a gyrus and the dura (“spread/fill-gyral”), and surrounding brainstem or cerebellar structures (“spread/fill-infratentorial”).

OCT Protocol and Data Processing/Analysis

Retinal imaging used spectral domain optical coherence tomography (SD-OCT, Spectralis, Heidelberg Engineering, Heidelberg, Germany). Peripapillary retinal nerve fiber layer (pRNFL) scans were obtained with the RNFL protocol, with an automatic real time (ART) of ≥60, using a 12.0° diameter circle centered on the head of the optic nerve. Macular scans were performed using a macular volume protocol, with a 20×20° field centered over the fovea, an ART of ≥16, and a signal-to-noise ratio of at least 25 dB.[21] Segmentation of the macular retinal nerve fiber layer (mRNFL), ganglion cell/inner plexiform layer (GCIPL), inner nuclear layer (INL), outer plexiform layer (OPL), outer nuclear layer (ONL), inner photoreceptor segment (IS), and outer photoreceptor segment (OS) was performed utilizing a validated, automated segmentation algorithm, as described previously.[22] Average macular thickness (AMT), a thickness measure of all retinal layers, was also measured. Average thicknesses were calculated within an annulus centered on the fovea, with an internal diameter of 1mm and an external diameter of 5mm. OCT methods and results are reported in agreement with consensus APOSTEL recommendations and scans were excluded if OSCAR-IB criteria were not met.[21, 23]

Statistical Analysis

Statistical calculations were performed using Stata 10.0 IC (StataCorp, College Station, TX, USA) and SAS version 9.4 (Cary, NC, USA). Raw volumes are reported for segmented brain structure volumes, but volumes normalized to intracranial volume were used for statistical comparisons. All OCT analyses utilized average values between the left and right eyes and were adjusted for confounding variables of optic neuritis history, age, sex, and use of disease modifying treatment for MS. Relationships between continuous variables were assessed by partial correlation testing. Simple group comparisons were performed with t-test or rank sum testing. A more robust comparison between participants with and without LME (both at baseline and longitudinal) was performed via linear mixed effects regression, using all data points, where participants were treated as a random variable, and predictors included time, LME, interaction between time and LME, and confounding variables. When possible, actual p values and/or confidence intervals are reported, or statistical significance is stratified into analyses that met thresholds of $p < 0.05$ or $p < 0.01$.

Results

Forty participants with MS were included, 35 of whom had > 1 visit available for longitudinal analyses. (Table 1). Twenty-six participants (65%) were female and 14 (35%) were male. Their mean age was 47.1 (SD 10.6) years and their mean disease duration was 12.0 (SD 8.7) years. Most of the participants had RRMS (75%) and most were on disease modifying therapy at the time of the baseline visit (67.5%). No contrast-enhancing WMLs were seen in any subject. Most participants had never experienced optic neuritis (72.5%).

Thirty-two (80%) participants had at least one focus of LME (Tables 1 and 2), with a median of 3.5 foci per subject (range 0 – 14). Participants with LME were older and less likely to have a diagnosis of PPMS (Table 1). Nodular foci were seen in 11 (28%) subjects and spread/fill foci were seen in 30 (75%) participants. Baseline cerebral and retinal imaging

findings are illustrated in Table 2. All participants had CLs, with a median count of 34 (range of 9–87) per subject. No difference was seen in the number or volume of CLs in those with or without LME. However, the total number of intracortical CLs was higher (6 (0–14)) in those with LME than without (3 (0–8), p=0.03). Hippocampal CL lesion count and volume was also significantly elevated in the LME + group. GCIPL and IS thicknesses and AMT were also significantly reduced in those with LME compared to those without.

Correlation between the retinal layer thicknesses and structural volumes, CL counts/volumes, and the number of foci of LME are shown in Table 3. INL thickness correlated with the number of spread/fill LME foci (p=−0.35, p=0.03) and ONL thickness correlated with spread/fill-sulcal count (r=−0.34, p=0.04). GCIPL thickness correlated with WML volume (r= −0.33, p<0.05). GCIPL had a stronger correlation, however, with total CL volume (r=−0.45, p < 0.01). GCIPL thickness and AMT both correlated with leukocortical lesion volume and GCIPL correlated with subpial lesion volume (r=−0.34, p=0.04).

The results of group comparisons for baseline retinal layer thicknesses in those with/without LME in a mixed models regression adjusted for covariates is shown in Table 4 and Figure 2. Baseline mRNFL was −4.598 μm thinner [−7.847, −1.349] in subjects with LME versus those without (p=0.01). A similar relationship was seen for GCIPL (−8.118 μm [−14.155, 2.081] thinner, p < 0.01) and AMT (−15.073 μm [−28.607, −1.540] thinner, p = 0.03) in those with LME. Baseline INL was −2.618 [−5.166, −0.071] μm thinner (p = 0.04) in participants with spread/fill LME foci at baseline. The presence of spread/fill-gyral LME at baseline was associated with baseline INL thickness that was −2.625 [−4.797, −0.452] μm thinner (p = 0.02) and OS thickness that was −1.786 [−3.411, −0.160] μm thinner (p = 0.03).

Longitudinal decline in layer thickness was seen for mRNFL, INL, IS, and OS in this cohort (Table 4), with the fastest decline seen for mRNFL (−0.910 μm/year [−1.295, 0.529], p < 0.01). Unexpectedly, GCIPL increased in this cohort over time (0.559 μm/year [0.036, 1.082], p = 0.04). The rate of decline in mRNFL was −1.113 [−1.974, −0.252] μm/year faster in those with spread/fill LME foci at baseline compared to those without (p=0.01; Figure 3). Similarly, IS declined −0.538 [−0.946, −0.130] μm/year faster in those with spread/fill LME at baseline compared to those without (p = 0.01). The presence of spread/fill-sulcal LME at baseline was associated with faster decline in mRNFL and OPL thickness (Figure 4), while the presence of spread/fill-gyral or spread/fill-infratentorial foci were not associated with any faster rates of thinning. INL thickness declined at a slower rate in those with spread/fill foci (1.409 [0.306, 2.513] μm/year slower) than the rate seen in those without (−1.506 μm/year [−2.454, −0.558], p < 0.01).

Discussion

The purpose of this study was to examine the relationship between meningeal inflammation, widespread neuronal loss, and focal lesion development by evaluating the interrelationship of LME and CLs with retinal layer thicknesses. Our results support a relationship between these complex aspects of MS pathology. These findings are in line with histopathologic data suggesting that leptomeningeal inflammation may be associated with initiation of local CL development and widespread neuronal degeneration.[5] Although LME was more commonly

seen in older subjects in this cohort, the relationship between retinal thinning and LME was independent of age and multiple other co-variates in mixed models regression, confirming a likely true biologic association.

We found baseline GCIPL thickness was reduced in patients with LME and GCIPL thickness inversely correlated with subpial and leukocortical CL volumes. These relationships may reflect global inflammation and neurodegeneration, though the case for implicating meningeal inflammation as a mediator of widespread retinal and cortical GM pathology, including subpial lesions, can be made. Subpial lesions are the most common CL found at autopsy and they do not originate in perivenular regions like WMLs.[1] Pathologically, meningeal B-cell follicles are found near subpial cortical lesions and appear to contribute to the progressive phenotype.[7] Meningeal lymphoid aggregates emit inflammatory cytokines that are involved in blood brain barrier breakdown, function as chemo-attractants for immune cells, and mediate organization of secondary lymphoid tissue.[24] Gradients of neuronal loss and demyelination are found emanating from meningeal follicles and imaging data shows a similar gradient of cortical thinning emanating from regions of LME.[8, 25] Animal models of this process confirm the development of subpial cortical demyelination and neurodegeneration after introduction of inflammatory cytokines into the subarachnoid space.[26] Further, the frequent location of subpial lesions in deep sulci suggest stagnant CSF as a mediator of local neuronal damage and demyelination. As the entire optic nerve is enveloped by meninges and bathed in CSF and significantly slower flow velocities are present in diseased optic nerves when compared to healthy controls,[27] we suggest that meningeal inflammation could be a mediator not only of the development of cortical GM pathology, but also optic nerve demyelination and retinal neurodegeneration – thus explaining the findings of our study.

In addition to finding a relationship between GCIPL thickness and LME, baseline GCIPL thickness inversely correlated with total CL and WML volume. Previous work shows that rates of GCIPL thinning are related to both whole brain and GM atrophy, seem to replicate global neurodegeneration, and are more robustly associated with progressive disease.[28] Our findings also replicate prior work demonstrating a relationship between GCIPL thinning and CL burden.[29] The relationship seen in this study between GCIPL thinning and CL burden is further supportive of a direct link between cerebral GM pathology and GCIPL thinning and is suggestive of a common pathway for cerebral neuronal loss and retinal ganglion cell loss.

Our findings of thinner mRNFL in those with LME at baseline and faster decline in mRNFL thickness in those with any type of LME or spread/fill type LME at baseline are also of particular interest. Thinning of the mRNFL is reported in patients with MS with and without a history of optic neuritis.[30] The RNFL of the macula represents the axons of retinal ganglion cells located in the GCIPL and can be damaged as part of the global neurodegeneration process in MS and locally via retrograde trans-synaptic axonal degeneration in optic neuritis or subclinical lesions.[31]

It is unclear why our data did not show any direct relationship between pRNFL and CLs or LME. pRNFL thinning occurs in patients with MS even in the absence of a history of ON and is thought to be due to subclinical loss of axons. Rates of change in pRNFL are

faster earlier in the disease process and slow with longer MS duration.[32] In our study, the mean disease duration was 12.0 years, which is typically after the pRNFL has decreased. Thus, the lack of correlations could be due to a 'basement effect' in pRNFL thinning. Also, reproducibility of pRNFL can be diminished in the setting of decreased signal and insufficient resolution, and this may have contributed to our lack of correlation in the setting of a small sample size. Similar noise in measurement could also be responsible for the unusual finding of increasing GCIPL thickness in the cohort over time. Progressive decline of this measure over time is a relatively consistent finding in most studies of retinal atrophy in MS.[13, 28] The expected declines seen in other layers (i.e. mRNFL) and the AMT seen in this study suggest that this is not indicative of a flaw in the OCT methods used. Rather, this may be an anomaly influenced by clinical/demographic factors of the subjects evaluated in this relatively small cohort. Confirmation of this work on a larger scale will be necessary both to replicate our findings for scientific validity and to investigate further the source of this finding.

Our findings in the INL do pose some questions, as the values of INL thickness were smaller in those with spread/fill LME foci at baseline, but faster declines in INL thickness were seen in those without LME. Historically, the INL has held an inconsistent place in MS pathology, as INL swelling has been associated with in vivo inflammatory disease activity, [33] but both INL and ONL thinning is seen at higher rates in MS, especially in those with progressive subtypes.[28]

Although we were able to identify a link between LME and retinal thinning in this study, a similar relationship between LME and CLs has been more difficult to demonstrate. In recent, similar studies, comparison in CL burden between those with and without LME either showed no difference[11] or a four-fold increase.[12] This cohort, which overlaps with our previous report,[11] confirmed prior findings of an association of hippocampal CLs and LME, but no relationship with overall CL burden. The inconsistent results in varying reports underlies difficulties in fully resolving CLs on MRI. CL burden on 7T MRI is quite protocol dependent[20] and subpial lesions are even underestimated when using 9T magnets.[20, 34] Given technological limitations in MRI, OCT represents an attractive tool to further evaluate the effect of meningeal inflammation on gray matter/neuronal pathology.

Similar to previous 7T studies,[11, 12, 16] our sample size is small, which limits the ability to find subtle relationships and for widespread applicability of the findings. Future work using 7T MRI should concentrate on multi-site data acquisition with unified protocols to work past this limitation. The small number of progressive MS subjects in this cohort inhibits any statistical comparison between progressive or relapsing forms of MS, which could be beneficial in gaining a greater understanding of the differences in the disease processes of MS subtypes. Such a comparison is of future interest, as the strongest relationships between meningeal inflammation and cortical demyelination and between LME and CLs seems to occur in SPMS.[7, 10]

Conclusion

This study provides support for a relationship between MRI findings of cortical pathology and LME and thinning of retinal layers as measured by OCT. Given prior data relating these imaging biomarkers to histopathology, our data may suggest that meningeal inflammation may be a common link resulting in widespread demyelination, neuronal loss, and axonal degeneration throughout the CNS and the retina. These findings should spur further work for replication and later evaluation of the use of OCT as an outcome measure in therapeutic trials targeting meningeal inflammation.

Acknowledgments

We wish to thank the OCT technicians at Johns Hopkins and the University of Maryland and the MRI technologists at the Kennedy Krieger Institute for their assistance in obtaining the data used in this study. We also wish to thank our research nurses and research coordinators for their tireless work in organizing and implementing study visits. We also thank members of Dr. Harrison's laboratory, including Seongjin Choi PhD, for assistance with image processing.

Funding

Funding for data acquisition for this study was provided by NIH/NINDS (1K23NS072366-01A1 and 1R01NS104403-01; to DH) and EMD-Serono (to DH). Time for data analysis was also supported by Race to Erase MS (to SS), Genentech (to SS), and National MS Society (RG-1606-08768 to SS).

Disclosures

RM, HC, and JL have no disclosures.

SS: Dr. Saidha has received consulting fees from Medical Logix for the development of CME programs in neurology and has served on scientific advisory boards for Biogen, Genzyme, Genentech Corporation, EMD Serono & Celgene. He is the PI of investigator-initiated studies funded by Genentech Corporation and Biogen Idec, received support from the Race to Erase MS foundation, and was the site investigator of a trial sponsored by MedDay Pharmaceuticals. He has received equity compensation for consulting from JuneBrain LLC, a retinal imaging device developer.

DMH: Dr. Harrison has received consulting fees from Genentech, EMD-Serono, Biogen, and Sanofi-Genzyme. Dr. Harrison has received research support from EMD-Serono and Genentech. Dr. Harrison has received royalties and writing fees for UpToDate, Inc. and the American College of Physicians.

MS Journal Appendix for MRI methodology

Hardware	
Field strength	7 Tesla
Manufacturer	Philips
Model	Achieva
Coil type (e.g. head, surface)	Head
Number of coil channels	Volume transmit, 32 channel receive
Other	Dielectric padding used to improve image homogeneity

Acquisition sequence		
Type (e.g. FLAIR, DIR, DTI, fMRI)	MPFLAIR	
Acquisition time	10:48	
Orientation	axial	
Alignment (e.g. anterior commissure/poster commissure line)	AP	
Voxel size	0.7mm isotropic	
TR	8000ms	
TE	400ms	
TI	2077ms	
Flip angle	90 degrees	
NEX	n/a	
Field of view	220 x 200 x 168	
Matrix size	316 x 251	
Parallel imaging	Yes	No
If used, parallel imaging method: (e.g. SENSE, GRAPPA)	SENSE	
Cardiac gating	Yes	No
If used, cardiac gating method: (e.g. PPU or ECG)		
Contrast enhancement	Yes	No
If used, provide name of contrast agent, dose and timing of scan post-contrast administration	Gadoteridol (Prohance), 0.1mmol/kg, ~20 minutes	
Other parameters:		

Acquisition sequence	
Type (e.g. FLAIR, DIR, DTI, fMRI)	MP2RAGE
Acquisition time	9:46
Orientation	sagittal
Alignment (e.g. anterior commissure/poster commissure line)	AP
Voxel size	0.7mm x 0.688mm x 0.688mm
TR	TRvolume = 8.25s TRTFE = 6.9ms
TE	1.97ms
TI	TI_1 = 1s TI_2 = 3.3s
Flip angle	FA_1 = 5° FA_2 = 5°
NEX	n/a
Field of view	220 x 220 x 144.2

Acquisition sequence		
Matrix size	316 x 316	
Parallel imaging	Yes	No
If used, parallel imaging method: (e.g. SENSE, GRAPPA)	SENSE	
Cardiac gating	Yes	No
If used, cardiac gating method: (e.g. PPU or ECG)		
Contrast enhancement	Yes	No
If used, provide name of contrast agent, dose and timing of scan post-contrast administration	Gadoteridol (Prohance), 0.1mmol/kg, ~10minutes	
Other parameters:		

References

1. Kidd D, Barkhof F, McConnell R, Algra PR, Allen IV, Revesz T. Cortical lesions in multiple sclerosis. Brain 1999;122 (Pt 1):17–26. [PubMed: 10050891]
2. Lucchinetti CF, Popescu BF, Bunyan RF, et al. Inflammatory cortical demyelination in early multiple sclerosis. N Engl J Med 2011;365:2188–2197. [PubMed: 22150037]
3. Harrison DM, Roy S, Oh J, et al. Association of Cortical Lesion Burden on 7-T Magnetic Resonance Imaging With Cognition and Disability in Multiple Sclerosis. JAMA Neurol 2015;72:1004–1012. [PubMed: 26192316]
4. Calabrese M, Rocca MA, Atzori M, et al. Cortical lesions in primary progressive multiple sclerosis: a 2-year longitudinal MR study. Neurology 2009;72:1330–1336. [PubMed: 19365054]
5. Kutzelnigg A, Lucchinetti CF, Stadelmann C, et al. Cortical demyelination and diffuse white matter injury in multiple sclerosis. Brain : a journal of neurology 2005;128:2705–2712. [PubMed: 16230320]
6. Howell OW, Reeves CA, Nicholas R, et al. Meningeal inflammation is widespread and linked to cortical pathology in multiple sclerosis. Brain 2011;134:2755–2771. [PubMed: 21840891]
7. Magliozzi R, Howell O, Vora A, et al. Meningeal B-cell follicles in secondary progressive multiple sclerosis associate with early onset of disease and severe cortical pathology. Brain 2007;130:1089–1104. [PubMed: 17438020]
8. Magliozzi R, Howell OW, Reeves C, et al. A Gradient of neuronal loss and meningeal inflammation in multiple sclerosis. Ann Neurol 2010;68:477–493. [PubMed: 20976767]
9. Absinta M, Vuolo L, Rao A, et al. Gadolinium-based MRI characterization of leptomeningeal inflammation in multiple sclerosis. Neurology 2015;85:18–28. [PubMed: 25888557]
10. Zivadinov R, Ramasamy DP, Vaneckova M, et al. Leptomeningeal contrast enhancement is associated with progression of cortical atrophy in MS: A retrospective, pilot, observational longitudinal study. Mult Scler 2017;23:1336–1345. [PubMed: 27811339]
11. Ighani M, Jonas S, Izbudak I, et al. No association between cortical lesions and leptomeningeal enhancement on 7-Tesla MRI in multiple sclerosis. Mult Scler 2019:1352458519876037.
12. Zurawski J, Tauhid S, Chu R, et al. 7T MRI cerebral leptomeningeal enhancement is common in relapsing-remitting multiple sclerosis and is associated with cortical and thalamic lesions. Mult Scler 2020;26:177–187. [PubMed: 31714181]
13. Saidha S, Al-Louzi O, Ratchford JN, et al. Optical coherence tomography reflects brain atrophy in multiple sclerosis: A four-year study. Ann Neurol 2015;78:801–813. [PubMed: 26190464]
14. Rothman A, Murphy OC, Fitzgerald KC, et al. Retinal measurements predict 10-year disability in multiple sclerosis. Ann Clin Transl Neurol 2019;6:222–232. [PubMed: 30847355]

15. Maranzano J, Dadar M, Rudko DA, et al. Comparison of Multiple Sclerosis Cortical Lesion Types Detected by Multicontrast 3T and 7T MRI. AJNR Am J Neuroradiol 2019;40:1162–1169. [PubMed: 31221631]
16. Harrison DM, Wang KY, Fiol J, et al. Leptomeningeal Enhancement at 7T in Multiple Sclerosis: Frequency, Morphology, and Relationship to Cortical Volume. J Neuroimaging 2017;27:461–468. [PubMed: 28464368]
17. Spini M, Choi S, Harrison DM. 7T MPFLAIR versus MP2RAGE for Quantifying Lesion Volume in Multiple Sclerosis. J Neuroimaging 2020;30:531–536. [PubMed: 32569408]
18. Polman CH, Reingold SC, Banwell B, et al. Diagnostic criteria for multiple sclerosis: 2010 revisions to the McDonald criteria. Annals of neurology 2011;69:292–302. [PubMed: 21387374]
19. Marques JP, Kober T, Krueger G, van der Zwaag W, Van de Moortele PF, Gruetter R. MP2RAGE, a self bias-field corrected sequence for improved segmentation and T1-mapping at high field. Neuroimage 2010;49:1271–1281. [PubMed: 19819338]
20. Beck ES, Sati P, Sethi V, et al. Improved Visualization of Cortical Lesions in Multiple Sclerosis Using 7T MP2RAGE. AJNR Am J Neuroradiol 2018.
21. Tewarie P, Balk L, Costello F, et al. The OSCAR-IB consensus criteria for retinal OCT quality assessment. PLoS One 2012;7:e34823. [PubMed: 22536333]
22. Lang A, Carass A, Hauser M, et al. Retinal layer segmentation of macular OCT images using boundary classification. Biomed Opt Express 2013;4:1133–1152. [PubMed: 23847738]
23. Cameron JR, Albrecht P, Cruz-Herranz A, Petzold A, Lagreze WA, Brandt AU. The APOSTEL recommendations for reporting quantitative optical coherence tomography studies. Neurology 2016;87:1960.
24. Serafini B, Rosicarelli B, Magliozzi R, Stigliano E, Aloisi F. Detection of ectopic B-cell follicles with germinal centers in the meninges of patients with secondary progressive multiple sclerosis. Brain Pathol 2004;14:164–174. [PubMed: 15193029]
25. Bergsland N, Ramasamy D, Tavazzi E, Hojnacki D, Weinstock-Guttman B, Zivadinov R. Leptomeningeal Contrast Enhancement Is Related to Focal Cortical Thinning in Relapsing-Remitting Multiple Sclerosis: A Cross-Sectional MRI Study. AJNR Am J Neuroradiol 2019;40:620–625. [PubMed: 30872420]
26. Gardner C, Magliozzi R, Durrenberger PF, Howell OW, Rundle J, Reynolds R. Cortical grey matter demyelination can be induced by elevated pro-inflammatory cytokines in the subarachnoid space of MOG-immunized rats. Brain 2013;136:3596–3608. [PubMed: 24176976]
27. Boye D, Montali M, Miller NR, et al. Flow dynamics of cerebrospinal fluid between the intracranial cavity and the subarachnoid space of the optic nerve measured with a diffusion magnetic resonance imaging sequence in patients with normal tension glaucoma. Clin Exp Ophthalmol 2018;46:511–518. [PubMed: 29178525]
28. Sotirchos ES, Gonzalez Caldito N, Filippatou A, et al. Progressive Multiple Sclerosis Is Associated with Faster and Specific Retinal Layer Atrophy. Ann Neurol 2020;87:885–896. [PubMed: 32285484]
29. Petracca M, Cordano C, Cellerino M, et al. Retinal degeneration in primary-progressive multiple sclerosis: A role for cortical lesions? Mult Scler 2017;23:43–50. [PubMed: 26993116]
30. Petzold A, Balcer LJ, Calabresi PA, et al. Retinal layer segmentation in multiple sclerosis: a systematic review and meta-analysis. Lancet Neurol 2017;16:797–812. [PubMed: 28920886]
31. Balk LJ, Petzold A. Current and future potential of retinal optical coherence tomography in multiple sclerosis with and without optic neuritis. Neurodegener Dis Manag 2014;4:165–176. [PubMed: 24832034]
32. Ratchford JN, Saidha S, Sotirchos ES, et al. Active MS is associated with accelerated retinal ganglion cell/inner plexiform layer thinning. Neurology 2013;80:47–54. [PubMed: 23267030]
33. Saidha S, Sotirchos ES, Ibrahim MA, et al. Microcystic macular oedema, thickness of the inner nuclear layer of the retina, and disease characteristics in multiple sclerosis: a retrospective study. Lancet Neurol 2012;11:963–972. [PubMed: 23041237]
34. Schmierer K, Parkes HG, So PW, et al. High field (9.4 Tesla) magnetic resonance imaging of cortical grey matter lesions in multiple sclerosis. Brain 2010;133:858–867. [PubMed: 20123726]

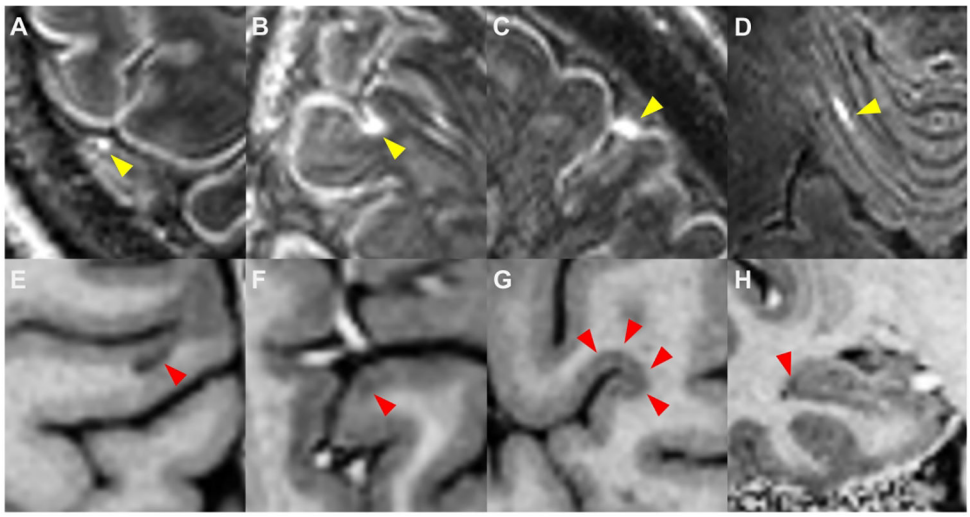

Figure 1: Leptomeningeal enhancement and cortical lesions.

Shown are examples of leptomeningeal enhancement (LME, yellow arrows) as visualized on 7T MPFLAIR and cortical lesions (red arrows) as visualized on T1-w images from 7T MP2RAGE (E – H). Four patterns of LME were noted: (A) nodular, (B) spread/fill-sulcal, (C) spread/fill-gyral, and (D) spread/fill-infratentorial. Four types of cortical lesion were also identified: (E) leukocortical, (F) intracortical, (G) subpial, and (H) hippocampal.

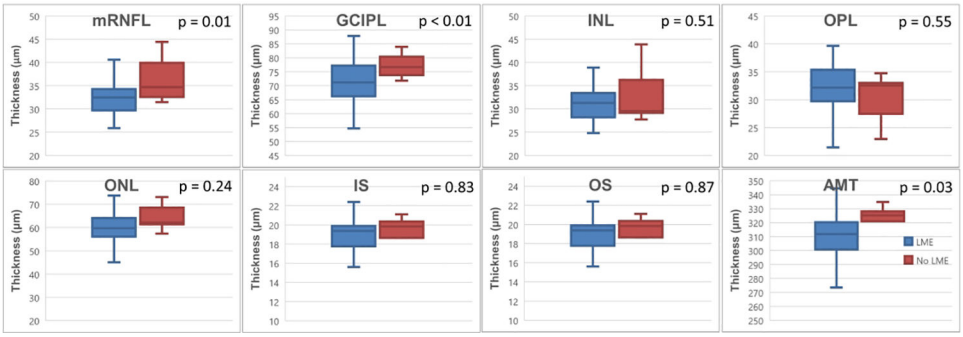

Figure 2: Distribution of baseline retinal layer thicknesses in those with/without leptomeningeal enhancement.

Boxplots showing distribution of values for baseline retinal layer thicknesses in the study cohort. LME: leptomenigneal enhancement; pRNFL: peripapillary retinal nerve fiber layer; mRNFL: macular retinal nerve fiber layer; GCIPL: ganglion cell layer + inner plexiform layer; INL: inner nuclear layer; OPL: outer plexiform layer; ONL: outer nuclear layer; IS: inner segment; OS: outer segment; AMT: average macular thickness.

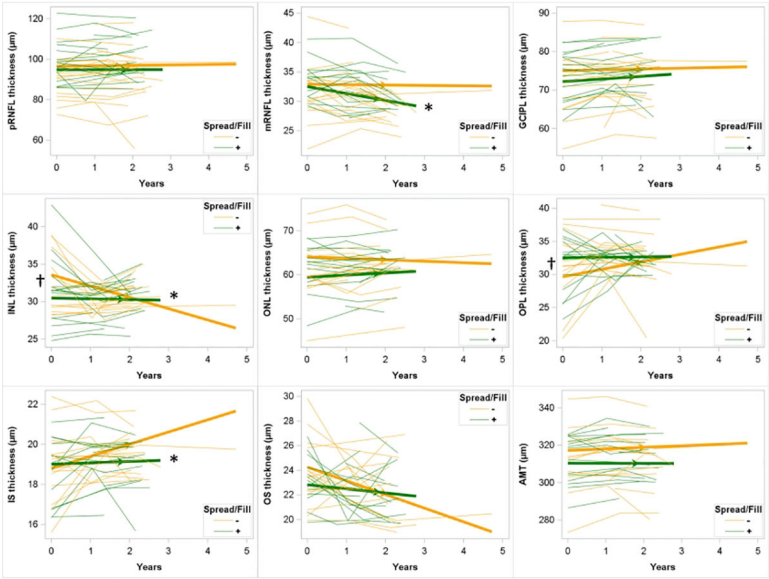

Figure 3: Longitudinal change in retinal layer thicknesses in those with and without spread/fill pattern leptomeningeal enhancement.

Spaghetti plots showing individual subject trajectories for retinal layer thicknesses. Thickened lines with arrows showing slope as determined by mixed models regression. Participants without spread/fill pattern leptomeningeal enhancement shown in yellow; those with shown in green. †: $p < 0.05$ for difference in baseline retinal layer thickness for those with spread/fill leptomeningeal enhancement compared to those without. *: difference in slope for those with spread/fill leptomeningeal enhancement compared to those without. LME: leptomenigneal enhancement; pRNFL: peripapillary retinal nerve fiber layer; mRNFL: macular retinal nerve fiber layer; GCIPL: ganglion cell layer + inner plexiform layer; INL: inner nuclear layer; OPL: outer plexiform layer; ONL: outer nuclear layer; IS: inner segment; OS: outer segment; AMT: average macular thickness.

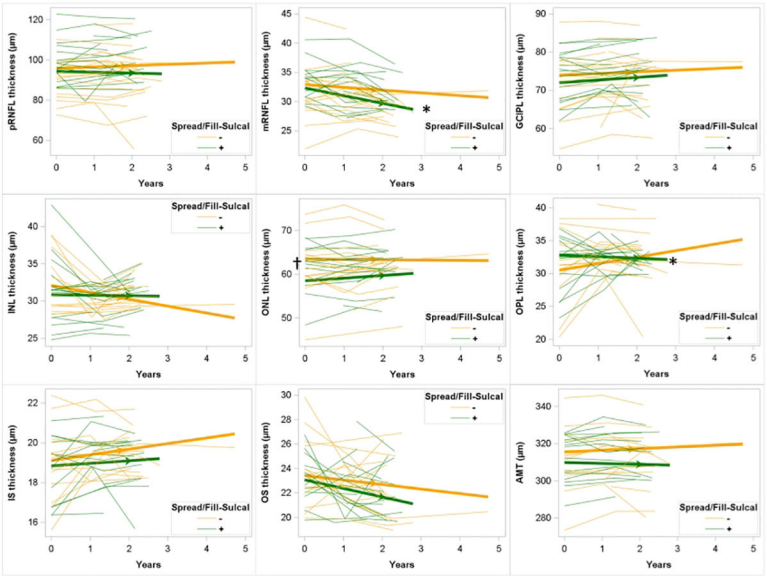

Figure 4: Longitudinal change in retinal layer thicknesses in those with and without spread/fill-sulcal pattern leptomeningeal enhancement.

Spaghetti plots showing individual subject trajectories for retinal layer thicknesses. Thickened lines with arrows showing slope as determined by mixed effects regression. Participants without spread/fill pattern leptomeningeal enhancement shown in yellow; those with shown in green. †: $p < 0.05$ for difference in baseline retinal layer thickness for those with spread/fill leptomeningeal enhancement compared to those without. *: $p < 0.05$ for difference in slope for those with spread/fill leptomeningeal enhancement compared to those without.

Table 1:

Demographics and clinical characteristics of study population.

Characteristic	All Subjects (n = 40)	LME + Subjects (n = 32)	LME – Subjects (n = 8)
Age (years), mean (SD)	47.1 (10.6)	49.1 (1.6)	39.1 (4.6) *
Female (%)	26 (65.0%)	10 (31.3%)	4 (50.0%)
Ethnicity • Not Hispanic/Latino • Hispanic/Latino • Unknown/Refused to Answer	 30 (75.0%) 1 (2.5%) 9 (22.5%)	 23 (71.9%) 1 (3.1%) 8 (25.0%)	 7 (87.5%) 0 (0.0%) 1 (12.5%)
Race • American Indian/Alaskan Native • Asian • Native Hawaiian/Pacific Islander • Black/African-American • White • More than one • Other • Unknown/Refused to Answer	 0 (0.0%) 0 (0.0%) 2 (5.0%) 30 (75.0%) 0 (0.0%) 2 (5.0%) 6 (15.0%)	 0 (0.0%) 0 (0.0%) 1 (3.1%) 24 (75.0%) 0 (0.0%) 2 (6.3%) 5 (15.6%)	 0 (0.0%) 0 (0.0%) 1 (12.5%) 6 (75.0%) 0 (0.0%) 0 (0.0%) 1 (12.5%)
MS Subtype • RRMS (%) • SPMS (%) • PPMS (%)	 30 (75.0%) 5 (12.5%) 5 (12.5%)	 25 (78.3%) 5 (15.6%) 2 (6.25%)	 5 (62.5%) 0 3 (37.5%) *
MS treatment name • No Treatment • Interferon-beta • Glatiramer acetate • Natalizumab • Teriflunomide • Fingolimod • Dimethyl fumarate	 13 (32.5%) 3 (7.5%) 6 (15.0%) 3 (7.5%) 1 (2.5%) 5 (12.5%) 9 (22.5%)	 10 (30.3%) 1 (3.0%) 6 (18.2%) 3 (9.1%) 1 (3.3%) 5 (15.2%) 7 (21.2%)	 3 (42.9%) 2 (28.6%) 0 0 0 0 2 (28.6%)
EDSS Score, median (Range)	3 (1–6.5)	3 (1 – 6.5)	2.25 (1 – 6)
Disease Duration (years), mean (SD)	12.0 (8.7)	13.2 (1.6)	7.3 (1.8)
Number of relapses in prior year	13 (32.5%)	11 (34.4%)	2 (25.0%)
Previous optic neuritis (n (%))	11 (27.5%)	10 (31.3%)	1 (12.5%)
Time period of follow up (years), median (range)	1.2 (0 – 4.7)	1.2 (0 – 2.8)	1.1 (0 – 4.7)

*: $p < 0.05$ for difference between subjects with leptomeningeal enhancement (LME +) and those without (LME −), by t-test or rank sum, as appropriate. SD: standard deviation; MS: multiple sclerosis; RRMS; relapsing-remitting multiple sclerosis; SPMS: secondary progressive multiple sclerosis; PPMS: primary progressive multiple sclerosis; EDSS: Expanded Disability Status Scale

Table 2:

Baseline imaging data. Median values shown, with range in parentheses.

Imaging Finding	All Subjects (n = 40)	LME + Subjects (n = 32)	LME – Subjects (n = 8)
Any LME focus count	3.5 (0–14)	4 (1 – 14)	N/A
Nodular LME focus count	0 (0–2)	0 (0 – 2)	N/A
Spread/fill LME focus count	3 (0–12)	3.5 (0 – 12)	N/A
Spread/fill-infratentorial LME focus count	0 (0–1)	0 (0 – 1)	N/A
Spread/fill-gyral LME focus count	2 (0–6)	2 (0 – 6)	N/A
Spread/fill-sulcal LME focus count	1 (0–10)	1 (0 – 10)	N/A
Total CL count	34 (9–87)	35 (10 – 87)	28 (9 – 51)
Total CL volume (mm^3)	429.1 (136.8–1224.3)	520.7 (136.8 – 1370.4)	370.9 (155.4 – 975.8)
Leukocortical CL count	24 (7–65)	24.5 (8 – 65)	19.5 (7 – 43)
Leukocortical CL volume (mm^3)	316.8 (68.9–790.6)	288.9 (68.9 – 790.6)	255.3 (95.8 – 786.3)
Intracortical CL count	6 (0–14)	6 (0 – 14)	3 (0 – 8)*
Intracortical CL volume (mm^3)	28.7 (0–115.0)	31.3 (0 – 115.0)	17.6 (0 – 42.7)
Subpial CL count	4 (0–13)	4 (0 – 13)	3 (0 – 6)
Subpial CL volume (mm^3)	134.0 (0– 708.7)	146.6 (0 – 708.7)	61.0 (19.9 – 254.1)
Hippocampal CL count	1 (0–7)	1 (0 – 7)	0 (0 – 2)*
Hippocampal CL volume (mm^3)	7.1 (0– 174.0)	9.1 (0 – 174.0)	0 (0 – 16.3)*
Cortical GM Volume (mm^3)	421256.1 (357884.9 – 512085.0)	417895.3 (363331.4 – 512085.0)	438726.4 (357884.9 – 488629.7)
WM Volume (mm^3)	487226.7 (402455.5– 593324.4)	483825 (402455.5 – 593324.4)	493106.0 (407799.0 – 541058.0)
WML Volume (mm^3)	2802.5 (51.7–19385.8)	2802.5 (51.7 – 19385.8)	3719.3 (831.0 – 15062.4)
pRNFL thickness (μm)	94.5 (61.3–122.8)	95.3 (61.0 – 123.0)	105.0 (91.0 – 119.5)
mRNFL thickness (μm)	33.4 (21.9–44.4)	32.7 (21.9 – 40.6)	34.7 (30.5 – 44.4)
GCIPL thickness (μm)	72.7 (54.7–87.8)	71.2 (54.7 – 87.8)	77.3 (71.8 – 84.0)*
INL thickness (μm)	31.0 (24.8–43.9)	31.4 (24.8 – 38.9)	29.5 (27.7 – 36.3)
OPL thickness (μm)	32.3 (20.4–39.7)	32.1 (20.4 – 38.3)	32.8 (27.5 – 39.6)
ONL thickness (μm)	61.4 (45.1–73.7)	59.8 (45.0 – 73.7)	61.4 (51.5 – 73.2)

Imaging Finding	All Subjects (n = 40)	LME + Subjects (n = 32)	LME – Subjects (n = 8)
IS thickness (μm)	19.4 (14.6–22.4)	19.4 (14.6 – 22.4)	20.1 (18.7 – 21.1) *
OS thickness (μm)	23.1 (19.3–29.9)	23.4 (19.3 – 29.8)	22.5 (19.5 – 25.1)
AMT (μm)	313.6 (273.5–344.6)	311.4 (273.5 – 344.6)	325.2 (309.7 – 334.9) *

* = p value < 0.05 for rank-sum difference between those with leptomeningeal enhancement (LME +) and those without (LME −). LME: leptomeningeal enhancing foci; GM: gray matter; WM: white matter; WML: white matter lesion; pRNFL: peripapillary retinal nerve fiber layer; mRNFL: macular retinal nerve fiber layer; GCIPL: ganglion cell layer + inner plexiform layer; INL: inner nuclear layer; OPL: outer plexiform layer; ONL: outer nuclear layer; IS: inner segment; OS: outer segment; AMT: average macular thickness.

Table 3:

Correlation between baseline values for retinal layer thicknesses with LME counts, cortical lesions, and brain segmentation values.

	pRNFL	mRFNL	GCIPL	INL	OPL	ONL	IS	OS	AMT
Any LME count	−0.26	−0.10	−0.25	−0.30	0.09	−0.32	−0.08	−0.21	−0.30
Nodular count	−0.26	−0.10	−0.27	0.16	−0.28	−0.15	−0.50 **†	0.23	−0.34 *
Spread/Fill count	−0.14	−0.08	−0.19	−0.35 *	0.17	−0.29	0.05	−0.27	−0.30
Spread/fill-infratentorial count	−0.04	−0.13	−0.07	−0.13	−0.07	−0.01	−0.10	0.17	−0.13
Spread/fill-gyral count	0.01	−0.01	−0.02	−0.24	0.11	−0.06	0.20	−0.17	−0.02
Spread/fill-sulcal count	−0.21	−0.08	−0.25	−0.31	0.17	−0.34 *	−0.06	−0.28	−0.27
Total CL Volume	0.21	−0.26	−0.45 **†	0.07	−0.06	−0.05	0.04	0.02	−0.34 *
Leukocortical CL count	−0.24	−0.15	−0.28	0.11	−0.18	−0.15	−0.22	−0.02	−0.37 *
Leukocortical CL volume	−0.16	−0.27	−0.41 *	0.19	−0.20	−0.01	−0.11	0.09	−0.35 *
Intracortical CL count	−0.26	−0.16	−0.32	0.11	−0.18	−0.14	−0.10	−0.01	−0.32
Intracortical CL volume	−0.24	−0.19	−0.32	0.16	−0.05	−0.01	0.17	−0.02	−0.24
Subpial CL count	−0.28	0.01	−0.30	−0.10	−0.03	0.02	0.05	−0.20	−0.19
Subpial CL volume	−0.21	−0.09	−0.34 *	−0.12	0.09	−0.06	0.12	−0.09	−0.21
Hypothalamic CL count	0.21	−0.28	0.07	−0.12	0.08	−0.17	0.11	−0.26	−0.13
Hypothalamic CL volume	0.18	−0.29	−0.03	0.01	0.20	−0.09	0.19	0.06	−0.10
WM volume	0.29	0.11	0.19	−0.22	0.05	−0.11	−0.01	−0.14	0.02
WML volume	−0.33	−0.24	−0.33 *	−0.03	−0.08	0.01	−0.21	0.16	−0.25
Cortical GM volume	−0.20	0.18	0.13	0.21	−0.03	−0.01	0.04	0.09	0.17

All correlations adjusted for covariates of age, sex, optic neuritis history, and use of disease modifying therapy. pRNFL: peripapillary retinal nerve fiber layer; mRNFL: macular retinal nerve fiber layer; GCIPL: ganglion cell layer + inner plexiform layer; INL: inner nuclear layer; OPL: outer plexiform layer; ONL: outer nuclear layer; IS: inner segment; OS: outer segment; AMT: average macular thickness; CL: cortical lesion: GM: gray matter; WM: white matter; WML: white matter lesion.

* p<0.05

** p<0.01

† p remained <0.05 after Bonferonni correction.

Table 4:

Effect of presence (+) or absence (−) of LME on retinal layer thicknesses at baseline and annualized rates of change.

	pRNFL		mRNFL		GCIPL		INL		OPL		ONL		IS		OS		AMT	
	Estimate	**p**	**Estimate**	**p**	**Estimate**	**p**	**Estimate**	**p**	**Estimate**	**p**	**Estimate**	**p**	**Estimate**	**p**	**Estimate**	**p**	**Estimate**	**p**
Annualized rate of change (μm/year)	0.130 (−0.725, 0.986)	0.77	−0.91 (−1.295, −0.529)	**<0.01***	0.559 (0.036, 1.082)	**0.04***	−0.513 (−1.006, −0.019)	**0.04***	0.439 −0.123 1.001	0.12	0.290 (−0.070, 0.651)	0.11	0.222 (0.041, 0.403)	**0.02***	−0.565 (−0.937, −0.193)	**<0.01***	0.273 (−0.570, 1.116)	0.52
LME (n, LME + = 32, LME − = 8)																		
Difference in baseline if present (μm)	−2.130 (−13.362, 9.103)	0.71	−4.598 (−7.847, −1.349)	**0.01***	−8.118 (−14.155, −2.081)	**<0.01***	−0.882 (−3.568, 1.803)	0.51	0.934 (−2.177, 4.048)	0.55	−3.059 (−8.188, 2.069)	0.24	0.129 (−1.061, 1.319)	0.83	−0.164 (−2.220, 1.891)	0.87	−15.073 (−28.607, −1.540)	**0.03***
Annualized rate of change absent (μm/year)	0.776 (−1.120 2.672)	0.42	−0.292 (−1.194, 0.610)	0.52	0.032 (−1.254, 1.317)	0.96	−1.075 (−2.217, 0.067)	0.06	0.566 (−0.718, 1.849)	0.38	0.040 (−0.875, 0.956)	0.93	0.344 (−0.091, 0.779)	0.12	−0.627 (−1.498, 0.244)	0.15	−0.136 (−2.236, 1.964)	0.90
Difference in rate of change present (μm/year)	−0.887 (−3.034, 1.261)	0.41	−0.734 (−1.734, 0.267)	0.15	0.667 (−0.751, 2.085)	0.35	0.749 (−0.526, 2.024)	0.24	−0.262 (−1.694, 1.169)	0.72	0.301 (−0.704, 1.305)	0.55	−0.173 (−0.654, 0.308)	0.47	0.104 (−0.866, 1.075)	0.83	0.380 (−1.930, 2.689)	0.74
Nodular (n, Nodular + = 11, Nodular − = 29)																		
Difference in baseline if present (μm)	−4.054 (−12.839, 4.732)	0.36	−1.135 (−3.857, 1.587)	0.41	−2.865 (−7.634, 1.906)	0.23	1.180 (−1.008, 3.367)	0.28	−1.815 (−4.311, 0.681)	0.15	−1.957 (−5.789, 1.876)	0.31	−1.064 (−1.919, −0.209)	**0.02***	1.131 (−0.432, 2.693)	0.15	−7.667 (−17.358, 2.024)	0.12
Annualized rate of change if absent (μm/year)	0.1085 (−0.94, 1.157)	0.84	−0.838 (−1.319, −0.356)	<0.01	0.531 (−0.126, 1.187)	0.11	−0.420 (−1.033, 0.193)	0.18	0.046 (−0.623, 0.715)	0.89	0.414 (−0.032, 0.861)	0.07	0.133 (−0.090, 0.357)	0.24	−0.519 (−0.979, −0.059)	**0.03***	−0.085 (−1.136, 0.966)	0.87
Difference in rate of change if present (μm/year)	−0.089 (−2.094, 1.915)	0.93	−0.196 (−1.065, 0.674)	0.65	0.126 (−1.076, 1.329)	0.83	−0.210 (−1.341, 0.921)	0.71	1.083 (−0.150, 2.315)	0.08	−0.429 (−1.242, 0.385)	0.30	0.234 (−0.176, 0.644)	0.26	−0.082 (−0.927, 0.764)	0.85	0.812 (−1.076, 2.700)	0.39
Spread/Fill (n, Spread/Fill + = 30, Spread/Fill − = 10)																		
Difference in baseline if present (μm)	−0.4265 (−11.342, 10.489)	0.94	−1.074 (−4.568, 2.419)	0.54	−4.694 (−10.767, 1.379)	0.13	−2.618 (−5.166, −0.071)	**0.04***	2.802 (−0.142, 5.747)	0.06	−4.354 (−9.195, 0.487)	0.08	0.174 (−0.955, 1.302)	0.76	−1.610 (−3.526, 0.305)	0.10	−9.026 (−22.273, 4.220)	0.18

	pRNFL		mRNFL		GCIPL		INL		OPL		ONL		IS		OS		AMT	
	Estimate	**p**	**Estimate**	**p**	**Estimate**	**p**	**Estimate**	**p**	**Estimate**	**p**	**Estimate**	**p**	**Estimate**	**p**	**Estimate**	**p**	**Estimate**	**p**
Annualized rate of change if absent (μm/year)	0.211 (−1.407, 1.829)	0.80	−0.065 (−0.808, 0.677)	0.86	0.215 (−0.882, 1.312)	0.70	−1.506 (−2.454, −0.558)	**<0.01***	1.126 (0.044, 2.208)	0.04	−0.332 (−1.078, 0.413)	0.38	0.606 (0.253, 0.959)	**<0.01***	−1.113 (−1.847, −0.378)	**<0.01***	0.822 (−0.926, 2.570)	0.35
Difference in rate of change if present (μm/year)	−0.184 (−2.126, 1.758)	0.85	−1.113 (−1.974, −0.252)	**0.01***	0.475 (−0.791, 1.740)	0.46	1.409 (0.306, 2.513)	**0.01***	−1.059 (−2.318, 0.201)	0.10	0.818 (−0.038, 1.673)	0.06	−0.538 (−0.946, −0.130)	**0.01***	0.779 (−0.076,1.633)	0.07	−0.869 (−2.881, 1.145)	0.39
Spread/fill-infratentorial (n, Spread/fill-infratentorial + = 4, Spread/fill-infratentorial − = 36)																		
Difference in baseline if present (μm)	3.234 (−12.201, 18.668)	0.68	−1.480 (−6.160, 3.200)	0.53	−2.859 (−11.102, 5.385)	0.49	−1.197 (−5.077, 2.684)	0.54	−1.440 (−5.837, 2.958)	0.51	−1.977 (−8.571, 4.617)	0.55	−0.653 (−2.218, 0.913)	0.41	1.684 (−1.001, 4.368)	0.21	−6.648 (−23.443, 10.148)	0.43
Annualized rate of change if absent (μm/year)	−0.024 (−0.930, 0.883)	0.96	−0.8512 (−1.262, −0.44)	<0.01	0.519 (−0.048, 1.087)	0.07	−0.544 (−1.071, −0.016)	**0.04***	0.362 (−0.233, 0.956)	0.23	0.261 (−0.130, 0.652)	0.19	0.207 (0.013, 0.401)	0.04	−0.563 (−0.964, −0.163)	**<0.01***	0.223 (−0.681, 1.126)	0.62
Difference in rate of change if present (μm/year)	2.795 (−1.809, 7.399)	0.23	−0.713 (−2.298, 0.871)	0.37	0.759 (−1.471, 2.989)	0.50	0.928 (−1.088, 2.944)	0.36	−0.023 (−2.295, 2.249)	0.98	0.360 (−1.174, 1.893)	0.64	−0.090 (−0.834, 0.655)	0.81	0.407 (−1.104, 1.918)	0.59	−0.889 (−4.384, 2.607)	0.61
Spread/fill-gyral (n, Spread/fill-gyral + = 27, Spread/fill-gyral − = 13)																		
Difference in baseline if present (μm)	−0.466 (−9.186, 8.254)	0.91	0.004 (−2.922, 2.930)	0.99	−3.258 (−8.300, 1.784)	0.20	−2.625 (−4.797, −0.452)	**0.02***	0.884 (−1.673, 3.44)	0.49	−2.691 (−6.720, 1.338)	0.19	0.302 (−0.652, 1.256)	0.53	−1.786 (−3.411, −0.16)	**0.03***	−7.751 (−18.324, 2.823)	0.15
Annualized rate of change if absent (μm/year)	−0.427 (−1.842, 0.987)	0.55	−0.352 (−1.018, 0.314)	0.29	0.489 (−0.476, 1.454)	0.31	−1.383 (−2.215, −0.550)	**<0.01***	1.105 (0.147, 2.063)	**0.02***	−0.160 (−0.818, 0.498)	0.63	0.540 (0.232, 0.848)	**<0.01***	−1.082 (−1.720, −0.443)	**<0.01***	0.679 (−0.843, 2.200)	0.37
Difference in rate of change if present (μm/year)	0.846 (−0.975, 2.667)	0.36	−0.816 (−1.632, 0.001)	0.05	0.119 (−1.055, 1.293)	0.84	1.381 (0.355, 2.407)	**<0.01***	−1.130 (−2.309, 0.049)	0.06	0.654 (−0.143, 1.450)	0.11	−0.502 (−0.878, −0.126)	**0.01***	0.818 (0.034, 1.602)	**0.04***	−0.761 (−2.613, 1.092)	0.41
Spread/fill-sulcal (n, Spread/fill-sulcal + = 22, Spread/fill-sulcal − = 18)																		

	pRNFL		mRNFL		GCIPL		INL		OPL		ONL		IS		OS		AMT	
	Estimate	**p**	**Estimate**	**p**	**Estimate**	**p**	**Estimate**	**p**	**Estimate**	**p**	**Estimate**	**p**	**Estimate**	**p**	**Estimate**	**p**	**Estimate**	**p**
Difference in baseline if present (μm)	−0.196 (−8.558, 8.166)	0.96	−0.521 (−3.129, 2.087)	0.69	−2.307 (−6.902, 2.288)	0.32	−1.228 (−3.288, 0.831)	0.24	2.204 (−0.135, 4.543)	0.06	−4.953 (−8.389, −1.517)	**0.005***	−0.204 (−1.059, 0.650)	0.63	−0.537 (−2.009, 0.935)	0.47	−6.523 (−15.866, 2.820)	0.17
Annualized rate of change if absent (μm/year)	0.647 (−0.613, 1.906)	0.31	−0.471 (−1.019, 0.077)	0.09	0.431 (−0.362, 1.224)	0.28	−0.923 (−1.645, −0.202)	**0.01***	0.991 (0.201, 1.78)	**0.01***	−0.075 (−0.606, 0.456)	0.78	0.282 (0.011, 0.553)	**0.04***	−0.371 (−0.926, 0.184)	0.19	0.872 (−0.351 2.096)	0.16
Difference in rate of change if present (μm/year)	−1.114 (−2.878, 0.651)	0.21	−0.838 (−1.608, −0.069)	**0.03***	0.264 (−0.835, 1.363)	0.63	0.861 (−0.142, 1.864)	0.09	−1.231 (−2.328, −0.134)	**0.03***	0.688 (−0.045, 1.421)	0.07	−0.152 (−0.527, 0.222)	0.42	−0.332 (−1.101, 0.437)	0.39	−1.386 (−3.097, 0.324)	0.11

Mixed models regression was performed, with intercepts, slopes, and interaction terms used for estimate. Regression performed included age, sex, history of optic neuritis, and use of disease modifying therapy as co-variates. Actual p values shown; those < 0 .05 indicated by "*" and in bold text. LME: leptomeningeal enhancing foci; pRNFL: peripapillary retinal nerve fiber layer; mRNFL: macular retinal nerve fiber layer; GCIPL: ganglion cell layer + inner plexiform layer; INL: inner nuclear layer; OPL: outer plexiform layer; ONL: outer nuclear layer; IS: inner segment; OS: outer segment; AMT: average macular thickness; μm: micrometer.